

Low-energy states, ground states, and variable frustrations of the finite-size dipolar Cairo latticesKseniia Makarova,^{1,2} Vladislav Strongin,^{1,2} Iuliia Titovets,¹ Aleksandr Syrov,¹ Ivan Zinchenko,^{1,2} Victor Samoylov ^{1,2}, Kevin Hofhuis ^{3,4}, Michael Saccone ⁵, Aleksandr Makarov ^{1,2,*}, Alan Farhan ^{4,6,†} and Konstantin Nefedev ^{1,2,‡}¹*School of Natural Sciences, Far Eastern Federal University, Vladivostok, Russky Island, 10 Ajax Bay, 690922, Russian Federation*²*Institute of Applied Mathematics, Far Eastern Branch, Russian Academy of Science, Vladivostok, Radio 7, 690041, Russian Federation*³*Laboratory for Mesoscopic Systems, Department of Materials, ETH Zurich, CH-8093 Zurich, Switzerland*⁴*Laboratory for Multiscale Materials Experiments, Paul Scherrer Institute, CH-5232 Villigen PSI, Switzerland*⁵*Physics Department, University of California, 1156 High Street, Santa Cruz, California 95064, USA*⁶*Department of Applied Physics, Aalto University School of Science, P.O. Box 15100, FI-00076 Aalto, Finland*

(Received 9 November 2020; revised 2 February 2021; accepted 16 March 2021; published 19 April 2021)

To investigate the influence of geometric frustration on the properties of low-energy configurations of systems of ferromagnetic nanoislands located on the edges of the Cairo lattice, the model of interacting Ising-like magnetic dipoles is used. By the method of complete enumeration, the densities of states of the Cairo pentagonal lattices of a finite number of Ising-like point dipoles are calculated. The calculated ground and low-energy states for systems with a small number of dipoles can be used to solve the problem of searching for the ground states in a system with a relatively large number of dipoles. It is shown that the ground-state energy of the Cairo pentagonal lattices exhibits nonmonotonic behavior on one of the lattice parameters. The lattice parameters can be used to control the degree of geometric frustration. For the studied lattices of a finite number of Ising dipoles on the Cairo lattice in the ground-state configurations, a number of closed pentagons is observed, which are different from the obtained maximum closed pentagons. The magnetic order in the ground-state configurations obeys the ice rule and the quasi-ice rules.

DOI: [10.1103/PhysRevE.103.042129](https://doi.org/10.1103/PhysRevE.103.042129)**I. INTRODUCTION**

A classic example, which is usually used to demonstrate the effect of frustration in condensed matter physics, is a system of three spins at the vertices of a triangle, interacting in pairs antiferromagnetically [1]. It is impossible to realize antiferromagnetic order over the entire triangle—at least two spins are ordered ferromagnetically and at least one connection will be inevitably frustrated. Understanding the physics of frustrations is essential to understanding the properties of many materials such as spin and macrospin glasses [2,3], water ice [4,5], spin ice and artificial spin ice [6–18], and many others.

Frustrations are often, but not always, observed in systems with slow relaxation, degeneracy, and, accordingly, a nonzero value of the residual entropy. Usually, in an ensemble with limited disorder, violations of local ordering rules manifest themselves in the form of localized excitations of low-energy states of the system [19–24]. Since frustrations give rise to various forms of the so-called forced disorder, it is quite natural that the disorder obeys some nontrivial rules, either locally or globally. The ice rule [24–27] and the quasi-ice rule [28] are well-known and important examples of local rules.

The influence of the geometry in combination with long-range interaction on thermodynamic states, on ordering

processes, degeneration of ground state, configurations and conformation of ground state, and local or global rules for establishing order (or for freezing disorder) is not an easy task as it might seem at first glance. The dipole-dipole interaction in artificial spin ice can significantly affect the formulation of the well-known ice rules according to which the local order is established. For example, for systems with a finite number of Ising dipoles on some lattices, not all states obeying the ice rule are ground states. In particular, it is easy to verify that the configuration of dipoles of square dipole ice with long-range dipole interaction is all “up” and all “to the right” is not a configuration of the ground state, although it satisfies the ice rule—at each node, “two inward, two out” [29].

The study of the thermodynamic states of bulk spin ice to investigate the phenomenon of frustration and to study in detail the configurations of bulk magnets is associated with well-known experimental difficulties. Therefore, researchers often prefer two-dimensional (2D) analogs for studying the statistical mechanics of Ising-like frustrated spin systems on lattices with specific geometry, including those not observed in nature [29–31].

Artificial spin ice systems with nonfixed, variable, but known coordination numbers are of particular interest. It is usually assumed that a change in the lattice parameters can significantly affect the degree of degeneracy of the energy levels and, accordingly, the low-temperature properties of the spin ice. Lattices with a variable coordination number were considered in Refs. [21–23,26].

Artificial spin ice is a prospective material from the point of view of practical applications for storing information since

*makarov.ag@dvfu.ru

†alan.farhan@gmx.net

‡knefedev@gmail.com

it potentially has a large information capacity. Other areas of application also include some sections of quantum electronics, as well as coding and storage of information [32]. The object of research, for example [33–36], is a two-dimensional array of ferromagnetic nanoislands elongated along one of the axes. The magnetic moments of such single-domain nanoparticles behave like Ising superspins. Their behavior can be described in terms of the Ising model. Natural spin ice and artificial spin ice, as well as spin and macrospin glasses [37–39], are extremely diverse systems with many realizations in nature. Their physics is too complex and varied, and they exhibit exotic properties and novel phenomena.

Spin or macrospin glasses are systems in which the translational invariance of the arrangement of atoms or nanoislands is violated. In contrast, systems of spin ice and artificial spin ice are characterized by the presence of translational invariance in the arrangement of the elements of the system. The study of the physics of spin glass has led to the emergence of new optimization algorithms, the development of a theory of computational complexity, made it possible to shed light on the processes of protein folding, as well as the development of a model of neural networks. Despite these and other successes, including in related branches of science, there are still several tough fundamental questions. These include the search for the ground-state configurations, which is common for spin glass and spin ice [39,40], revealing the nature of the ground state [41,42], degeneration of the ground state [43,44], and others.

There are many approaches to obtaining an approximate solution of the Ising model; see, for example, [17,30,45–49]. The exact calculation of the ground-state energy even for a classical Ising spin glass on a 2D lattice with the nearest-neighbor interaction is a computationally difficult problem, or even NP-complete [41]. It is believed that the issue of searching for the configuration of the ground state of a spin glass in the general case is a problem of the NP class [40]. Finding the ground state for spin ice even in a simple model of Ising-like dipoles is associated with combinatorial optimization problems. In Ref. [50], the model of Heisenberg-like dipoles is considered, which can even have small oscillations relative to the direction distinguished by the shape anisotropy. This additional degree of freedom can be considered as an additional possibility for excitations, and in the presence of chaos in the directions of the magnetic moments, the algorithmic complexity of the problem under study increases intractably.

The combinatorial optimization problems that arise when calculating the ground state of a spin glass and spin (macrospin ice) system are similar, and it should be noted that the solution to these problems is as difficult as they are of fundamental and practical interest.

II. MODEL AND COMPUTATIONAL METHODS

The Cairo lattice is sometimes called the “pentagonal lattice” [51] or “Cairo pentagonal lattice” [52–54]. The literature [55–58] argues that geometric frustrations in the Cairo lattice can lead to exotic properties and a variety of degenerate ground states. The path to the ground state in magnetically frustrated systems is an interesting optimization question that can be attempted using various approaches. For example, in geometrically frustrated artificial kagome spin ice, Monte

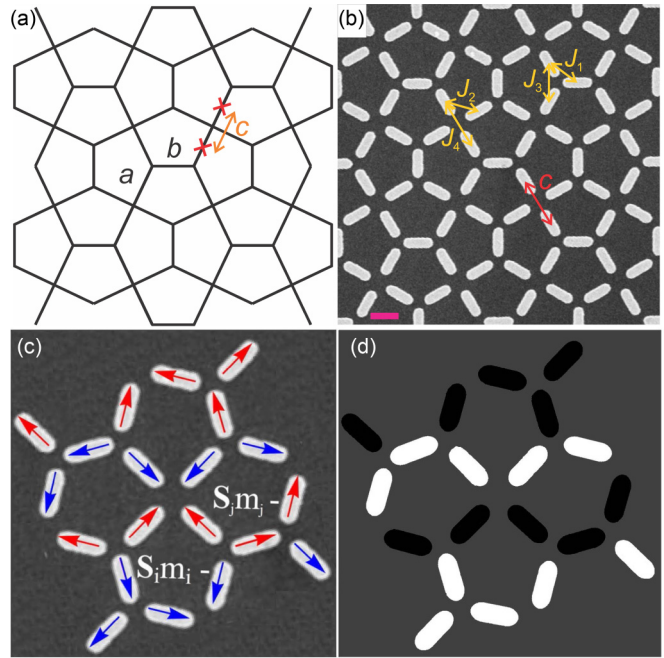


FIG. 1. (a) Cairo lattice and its relevant parameters a and b representing the two site lengths, while c (highlighted by an orange double arrow) represents the distance between collinear dipoles (red crosses) meeting at four-dipole vertices. (b) Scanning electron microscopy (SEM) image of a dipolar Cairo lattice consisting of nanoislands of lengths $L = 300$ nm and widths $W = 100$ nm, placed on the edges of the Cairo lattice with lattice parameters $a = 472$ nm, $b = 344$ nm, and $c = 500$ nm. Interactions are presented between nearest neighbors in the short-range model. (c) The explanation of the used Ising-dipoles model, where $S_i m_i$ —magnetic moments and S_i —unite the one-component vector of magnetic moment. (Red arrows) “spin up” ($|S_i| = +1$); (blue arrows) “spin down” ($|S_i| = -1$). For this configuration of $N = 20$ dipoles, the spin excess $\mathbf{M} = \sum_i^N |S_i| = 0$. (d) The gray-scale representation of the magnetic moments configuration, $|S_i| = +1$ (black), $|S_i| = -1$ (white), is presented to compare with experimental XMCD data [63].

Carlo methods, employing the so-called dumbbell model [59–61] were used to predict thermodynamic phase transitions towards a long-range ordered ground state, which have also been experimentally confirmed [62].

In our paper, we calculate the ground-state configuration in frame long-range interaction model and estimate the degree of frustration of samples of a finite quantity of dipoles of the Cairo lattice for a given lattice parameter, i.e., a given coordination number. Based on this analysis, we have attempted to predict the configuration of the ground state of pentagonal lattices when there are a relatively large number of dipoles. The results in Ref. [63] present an experimental study of two-dimensional artificial spin ice, where Ising-like nanoislands are placed on the centers of the edges of the so-called Cairo lattice (see Fig. 1).

Figures 1(a) and 1(b) show the lattice parameters a , b , and c . With this notation the calculations were performed for $a = 472$ nm, $b = 344$ nm, and various values of c , as in Ref. [63], with the only difference that we calculated the properties of the ground states for $c > 600$ nm. Since the

sizes of the nanoislands are below the critical threshold for a single-domain state, and the shape anisotropy highlights the direction for the magnetic moment, we investigated the model of Ising-like point dipoles. For clarity and presentation of our model, we calculated the centers of the nanoislands and placed the lattice of point dipoles on the lattice shown in the image obtained in Ref. [63] by scanning electron microscopy (SEM) [Fig. 1(b)]. The Cairo dipole lattice sample consisted of nanoislands with lengths and widths of 300 nm and 100 nm, respectively. In Fig. 1(c), arrows show one of the possible configurations of the 20-dipole array, while the corresponding XMCD contrast is given in Fig. 1(d).

The energy of the dipole-dipole interaction in the Cairo lattice was calculated using the following well-known formula:

$$E_{ij} = \frac{(\mathbf{m}_i \mathbf{m}_j)}{|\mathbf{R}_{ij}|^3} - 3 \frac{(\mathbf{m}_i \mathbf{R}_{ij})(\mathbf{m}_j \mathbf{R}_{ij})}{|\mathbf{R}_{ij}|^5}, \quad (1)$$

where $\mathbf{m}_i = \mu_i \mathbf{S}_i m_i$ is the moment of the i dipole, $\mu_i = M_s V$ is the value of the magnetic moment of the nanoisland with a volume V , the saturation magnetization M_s , and $\mathbf{R}_{ij} = l \mathbf{r}_{ij}$ is the radius vector connecting the dipoles i and j , and l is the factor which has length dimension. Then,

$$E_{ij} = D \mathbf{S}_i \mathbf{S}_j \left[\frac{(m_i m_j)}{|\mathbf{r}_{ij}|^3} - 3 \frac{(m_i \mathbf{r}_{ij})(m_j \mathbf{r}_{ij})}{|\mathbf{r}_{ij}|^5} \right], \quad (2)$$

where $D = \mu_i \mu_j / l^3$ is the dimensional constant for the dipole interaction. Therefore, the energy of all pair interactions E/D in this research has a dimensionless value. A lattice with free boundary conditions was used, in which Ising-like point dipoles $\mathbf{S}_i m_i$ are placed on the edges of the pentagons.

The direction of a magnetic moment is defined by $\mathbf{S}_i m_i = \mathbf{S}_i \{m_x, m_y, m_z\}$, where \mathbf{S}_i is the unit one-component vector of the magnetic moment and defines the direction “up” or “down”, i.e., $|\mathbf{S}_i|$ can have only two values of its component $+1$ or -1 . In Fig. 1(c), the corresponding $\mathbf{S}_i m_i$ are indicated by arrows, and the color corresponds to the sign of $|\mathbf{S}_i|$, conditionally, blue—“down”, or red—“up”. The gray-scale representation for the moments configuration is shown in Fig. 1(d). The projection of the magnetic moments on a given direction of $|\mathbf{S}_i|$ allows us to obtain a black-white image of the spin configuration similar to experimentally obtained XMCD images. The direction is chosen so that there are no vectors orthogonal to this direction. Here it is chosen along the x direction [0 degrees for the example given in Fig. 1(d) with a 17-degree lattice rotation), in order to obtain the same black-white pattern as experiments. The moments of the nanoislands [see Fig. 1(c)] will have nonzero values of both components if the entire lattice is rotated by a certain angle entirely, except for when the direction is parallel to one of the four subsets of moment vectors (0, 60, 90, or 120 degrees plus the lattice rotation).

It is possible to introduce the “spin excess”:

$$M = \sum_{i=1}^N S_i, \quad (3)$$

the difference between magnetic moments “up” and “down” for each configuration. Here and after we will omit the signs of the vector and module for S_i , because it has one component. Nevertheless, it should be remembered that the value of M will

depend on the choice of the axis (direction) on which the S_i vectors are projected. Therefore spin excess M in our research has a dimensionless value.

There are 2^N configurations in an Ising model consisting of N dipoles. The uniqueness of the configuration of the magnetic moments is coded by a single set $\{S_i\}$, in fact this is the “ID” of the magnetic moments configuration. The orientation of the magnetic moment is determined by the direction of the easy axis of the nanoislands’ magnetization, which is controlled in this case by the shape anisotropy. Based on SEM data [see Fig. 1(b) [63]], the nanoislands are seemingly identical, while around 5% disorder in the form of a Gaussian is often used in past kinetic Monte Carlo simulations to match experimental observations [64]. As a result, for each configuration of dipolar moments in the Ising model we can match the spin excess M and in the case of “all-to-all” dipolar interaction the total energy,

$$E = \sum_{(i,j)} E_{ij} = \sum_{i=1}^N \sum_{j=i+1}^{N-1} E_{ij}. \quad (4)$$

Moment configurations with the smallest calculated energy E are branded as the “ground states.” For the frustrated system with an Ising model, from geometry or lattice, even in the ground state, there can be multiple degenerated. In the ground state, there are pair interaction energies E_{ij} that are unfavorable (i.e., similar to other frustrated systems like the kagome system [65]). This means that there are more possible states with a ground-state energy, and, more important, that there is a special lowest energy value,

$$E_{\min} = - \sum_{(i,j)} |E_{ij}|, \quad (5)$$

which is even lower than the ground-state energy, but it is not realized. Despite the fact that there is no such set of $\{S_i\}$ that would correspond to the value of E_{\min} , the knowledge of this hypothetical energy level for a frustrated system can be very useful for assessing the degree of frustration (relative numbers of excited pairs of moments). Another useful characteristic of systems with frustration is the value,

$$E_{\max} = \sum_{(i,j)} |E_{ij}| = -E_{\min}. \quad (6)$$

All permitted energy values for any physical system with pair interactions are always in the range from E_{\min} to E_{\max} . For frustrated systems, the ground-state (gs) energy usually has a higher value than the minimum value $E_{\text{gs}} > E_{\min}$. The exotic thermodynamic properties of frustrated systems will depend not only on the type of the distribution of states, but on the location of the energy spectrum within the interval (E_{\min}, E_{\max}) .

A quantitative measure of the frustrations was introduced in Ref. [17] and here it is calculated as the relative number of excitations in the ground state using

$$P_f(T) = \frac{E_{\max} + \langle E \rangle(T)}{2E_{\max}} = \frac{E_{\max} + E_{\text{gs}}}{2E_{\max}} \Big|_{T \rightarrow 0}, \quad (7)$$

where $P_f \in [0, 1]$ and $\langle E \rangle(T)$ is the thermodynamic mean value. For 1D, 2D, and 3D Ising ferromagnets $P_f(T \rightarrow 0) = 0$, and there are no frustrations.

We used the complete enumeration method for lattices with $N = 20$ and 40 dipoles. The time it takes to solve a problem by the complete enumeration method increases exponentially with the number of elements in the model. However, the benefits of this method include the fact that if it is possible to apply this method, it always finds a solution.

The search for the ground state for an 80-dipole lattice was performed in two ways. First, we calculated all possible states of the lattices with $N = 20$, then from the low-energy states we collected the low-energy state for the Cairo lattice with $N = 80$. We used less than 0.1% of the low-energy states to combine the four found low-energy states of 20 dipoles into a lattice of 80 dipoles. Secondly, using the hybrid multispin Monte Carlo method [17], the ground state was sought for the 80-dipole lattice.

The method consists of combining the classical Monte Carlo and the complete enumeration method. The explanation of a common scheme was given in Ref. [17]. We proposed a new hybrid multispin method (the logical continuation of the Metropolis algorithm [45]), which in some cases can be used to solve the problem of ground-state or low-energy state search for frustrated vector models of complex systems of many interacting Ising dipoles. We used Eqs. (1) and (4).

The idea was as follows: A region from 10 to 23 nearest-neighbor and close-neighbor (up to the fifth coordination sphere) dipoles were randomly selected. For this area, a complete enumeration was performed taking into account the general distribution of internal energy in the “all-to-all” interaction model with free boundary conditions for the configuration as a whole and formula (1). The energy and configurations of the ground state for this local region were calculated, after which all moments were brought to the state with the lowest energy, and we randomly changed the area to decrease the energy. In the Metropolis algorithm, at $T \rightarrow 0$, the probability of accepting the configuration with the lowest energy tends to unity. If there was a degeneration of local ground states, we randomly chose any gs configuration with uniform probability from the set of those found.

III. RESULTS

We have calculated 2^{20} states for a system of $N = 20$ spins with the parameters of the Cairo pentagonal lattice specified in Ref. [63] for the case of free boundary conditions. Figure 2 shows DOS projections $g(E, M)$ onto the (E, M) plane, where M is the spin excess or the difference between the number of spins “up” or “down.”

The lower axis of each of Figs. 2(a)–2(d) corresponds to the minimum value of the interaction energy of the dipoles E_{\min} , calculated by formula (5). The upper axes of Figs. 2(a)–2(d) correspond to the maximum value of the energy of dipole-dipole interactions E_{\max} , formula (6). The distance between the minimum of the energy E_{\min} and the ground state E_{gs} is the “band gap” or “energy gap.” There are no energy levels in the energy gap since configurations with such an energy do not exist. One of the distinguishing features of frustrated systems is that their band gaps are located below the ground state. Due to the structure of the Hamiltonian, the interaction law, or the peculiarities of the lattice geometry, states with fewer excitations than in the ground state do not exist. Thus,

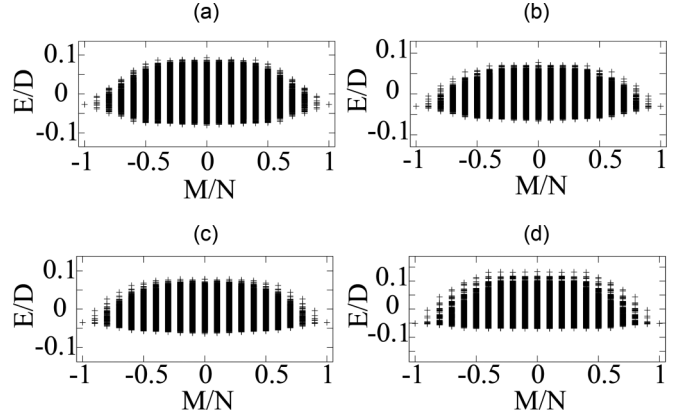


FIG. 2. Projection of the density of states onto the plane (E, M) for the Cairo lattices of $N = 20$ dipoles, $c = 376, 450, 500, 600$ nm, respectively, for (a)–(d).

the lowest energy states of the studied Cairo lattices, even the ground states realized at $T \rightarrow 0$, always contain excitations of pair interactions of the “head to head” or “tail to tail” type. As can be seen from Figs. 2(a)–2(d), the energy gap increases with increasing c .

Figure 3(a) shows the density of states for the $N = 20$ dipole system, $c = 376$ nm. In Fig. 3(a) the distribution of degeneration of configurations $g(E, M)$ is presented. Figure 3(b) shows the low-energy part of $g(E, M)$ starting from the fourfold degenerate ground state. The function $g(E, M)$ does not increase

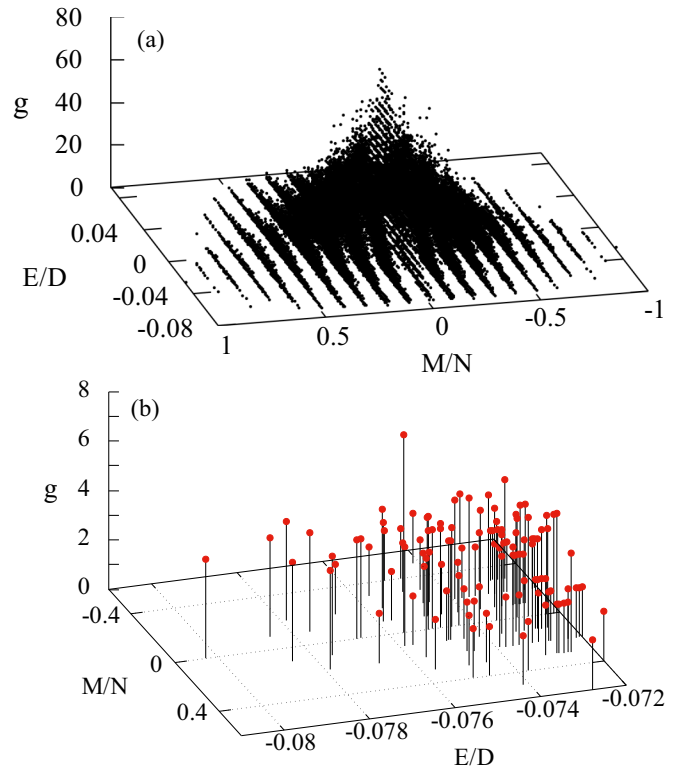


FIG. 3. (a) The quantity of states $g(E, M)$ for the Cairo lattices of $N = 20$ dipoles, $c = 376$ nm. (b) Low energy part of $g(E, M)$ for $c = 376$ nm.

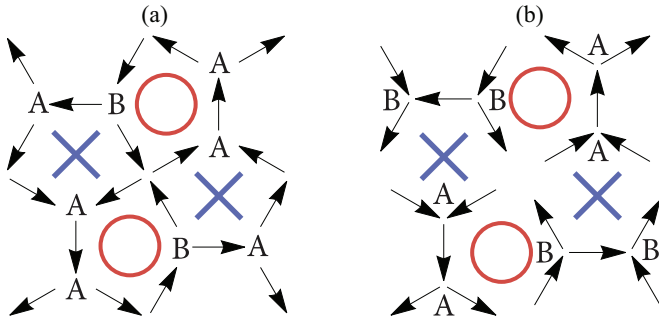


FIG. 4. (a) One of four ground-state configurations for lattices $N = 20$ with $c = 376$ nm, 450 nm, 500 nm. (b) One of four configurations for lattice $N = 20$ with 600 nm.

sharply with an increase in internal energy from the ground state to low-energy configurations. In the case of a dipole-dipole interaction, the degeneracy reaches a maximum density in the area of $g(0, 0)$. The maximum values of the energy degeneracy over the spin excess at the selected accuracy are observed for the following function $g(-0.00326, 0) = g(0.00143, 0) = g(0.00721, 0) = 80$.

Note here that all the configurations of the ground state that we found in this work obey ice rule “two in–two out” for nodes of four dipoles, and the kagome ice rules “two in–one out” or “two out–one in” for nodes of three dipoles. Figure 4 shows the ground states for the studied lattices of 20 dipoles with free boundary conditions and different values of the lattice parameter $c = 376, 450, 500,$ and 600 nm. As seen in Fig. 4, the ground states for the lattice of dipoles with $c = 376, 450,$ and 500 nm are the same and differ from the ground states of the lattice where $c = 600$ nm only by inverted angular dipoles. We marked with a red circle the pentagons in which all the dipoles are lined up according to the “head-to-tail” rule. With a cross, we marked the pentagons in which, for nearest neighbors, at least one violation of the “head-tail” rule takes place, respectively; frustrations of pair interactions were observed in these figures.

Obtained in the long-range model the candidate ground state could be analyzed in the frame of the short-range model. The paper [63] used notations for a short-range model, with the explanation of pair interactions given in Fig. 1(b). The Type-A vertex minimizes (satisfies) both J_1 interactions, while J_3 is maximized (Fig. 4). The Type-B vertex satisfies J_1 and the J_3 interactions, while maximizing the other J_1 .

It should be noted that there are configurations for a lattice of 20 dipoles in which all four pentagons (relative to the central cross) have no violations of the “head-tail” rule (for nearest neighbors). These configurations have energies higher than the ground state. In these states, the ice rule and the quasi-ice rule are fulfilled. The dipole-dipole interaction removes the strong degeneracy of the low-energy states of the dipole Cairo ice.

The four same ground states were calculated by means of complete enumeration for each Cairo lattice of 20 dipoles with parameters $c = 376, 450$ nm, 500 nm [Fig. 4(a)]; for $c = 600$ nm one ground-state configuration is presented in Fig. 4(b).

Figure 5 shows one of the excited states of a system of 20 dipoles on a pentagonal lattice for $c = 376$ nm. We give it

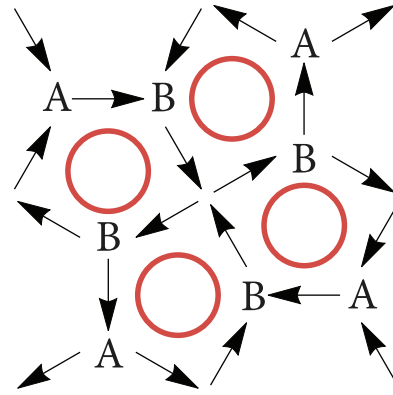


FIG. 5. One of the excited states for a system of 20 dipoles, $c = 376$ nm.

as an example to show that in the long-range dipole interaction model, there are excited non-ground-state configurations, where the ice rules and the quasi-ice rules are fulfilled, as well as for all four completely closed pentagons where the “head-tail” rule is fulfilled. It is possible to see, that in the ground-state configuration in Fig. 4(a), there are more Type-A vertices, than in excited states, for example, in the state in Fig. 5.

The energies and configurations of the ground states for the Cairo pentagonal lattice, consisting of 40 dipoles, were calculated by the complete enumeration method. It was found that, as in the case for $N = 20$, for a system of 40 dipoles, the configurations of the ground state for $c = 376, 450,$ and 500 nm are repeated. The configuration of the ground state of the lattice with $c = 600$ nm differs from the configuration of the ground state for lattices with other values of c only in that the moments at the corners of the lattice have other directions.

The exactly calculated ground-state configurations of the Cairo lattice of 40 dipoles were used to test the solutions that were obtained by way of combining low-energy states. In addition, they were used to check the performance of the solutions obtained by the Monte Carlo method. The combination method consisted of building the configuration of the ground state of the large pentagonal lattice of dipoles using the known low-energy configurations of Cairo lattices with fewer dipoles. Suppose a lattice with N dipoles consists of two subsystems, into which it is equally divided. Each of the subsystems will have $2^{N/2}$ configurations. Each ground state of a lattice of N dipoles will be constructed from two configurations of these two subsystems. These two configurations will be in the $2^{N/2}$ space. In this case, it is easy to verify that these will necessarily be low-energy configurations, the excitations of which will be associated only with the effect of boundaries.

All possible configurations of the Cairo lattice of 20 spins were sorted in order of increasing energy and the densities of states were plotted [see Figs. 2(a)–2(d)]. In Fig. 6 we have depicted a small number of low-energy states of the investigated lattices.

Figure 6 shows the projections of the density of states onto the (E, M) plane of low-energy configurations for $c = 376, 450, 500, 600, 650,$ and 700 nm, respectively, for Figs. 6(a)–6(f). Calculations were performed for $N = 20$ dipoles. The circles denote configurations that were part of the

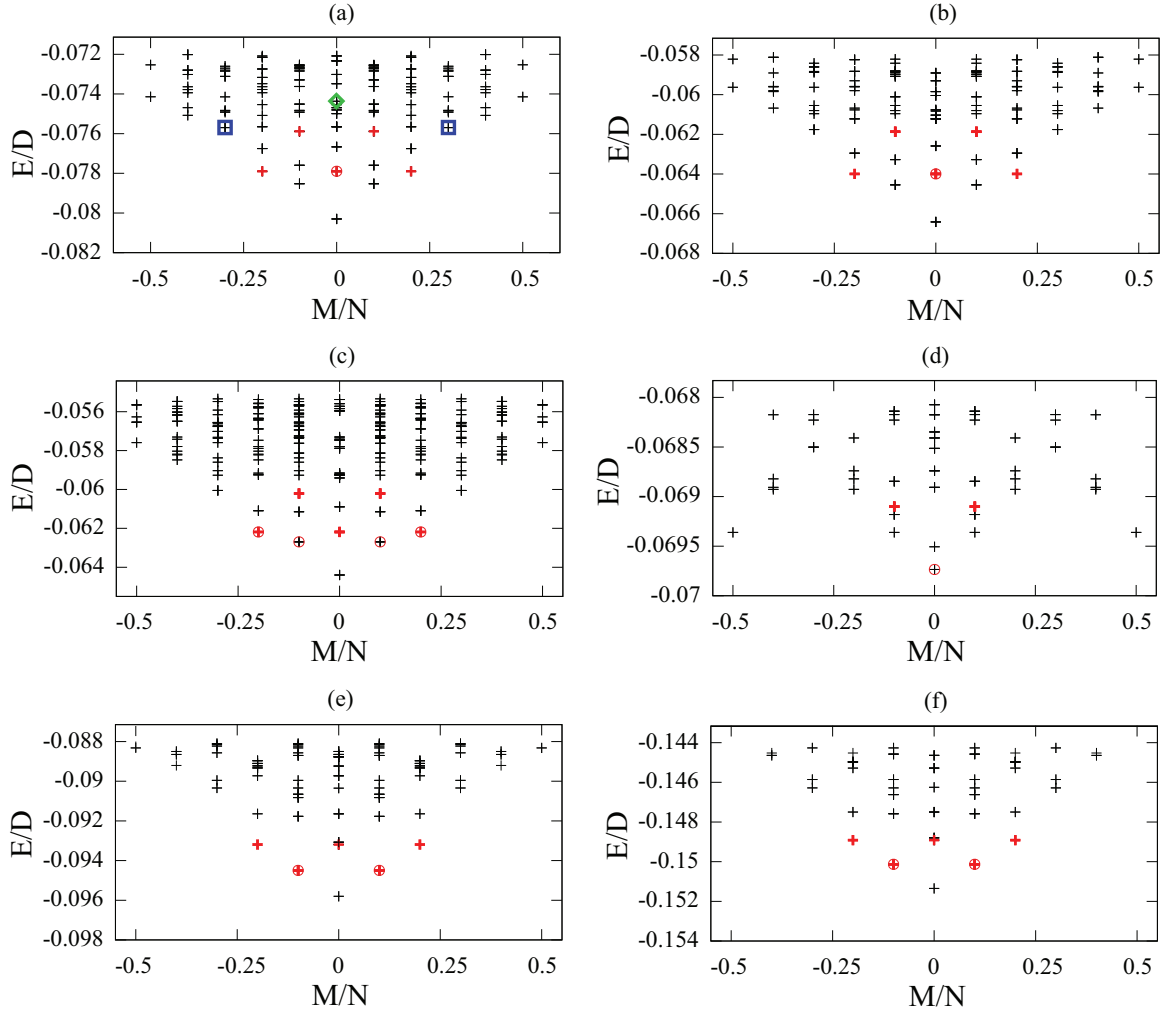


FIG. 6. Reduced DOS for lattices $N = 20$ with $c = 376, 450, 500, 600, 650,$ and 700 nm, respectively, for (a)–(f). The circles indicate the states of the subsystems from which the ground state for a system of 40 dipoles is constructed. A bold red cross denotes the states from which the lattice states of 80 dipoles were constructed. In (a), the green rhombus indicates the excited state with the maximum number of closed pentagons. The excited state for $N = 40$ was collected from the states indicated by the blue squares.

ground-state configurations for the Cairo lattice of 40 dipoles with the corresponding value of the parameter c . It is easy to see that only for a lattice of 40 dipoles, where $c = 600$ nm, the configurations of two subsystems are the ground states for a lattice of 20 dipoles. For the remaining lattices, the states of subsystems of 20 dipoles, from which the states of 40 dipoles were constructed, are excited, albeit low-energy states. Obviously, the boundary effect plays a role here. For lattices with $c = 376, 450,$ and 500 nm, the energy of interactions by absolute value at sites with four nearest neighbors can be more than at sites with three nearest neighbors. Lattices with $c = 600, 650,$ and 700 nm decay into sublattices of five spins each, so the total interaction between the subsystems weakens. The states of the subsystems of 40 dipoles for $c = 650$ and 700 nm are also excited due to the boundary spins. It should be noted that the ground state of a system of 40 dipoles at $c = 650$ and 700 nm can be constructed only from configurations of 20 dipoles, which are most close to the ground state [see the circles in Figs. 6(e) and 6(f)]. A characteristic feature of the space of states for the selected values of parameter c is that there are some critical values of this parameter where

the positions in the (E, M) space of the configurations, from which the ground states of 40 and 80 dipoles are constructed, no longer change; see, for example, Figs. 6(a) and 6(b), and also Figs. 6(e) and 6(f). In Fig. 6(a), we have highlighted the energy and spin excess of the state shown in Fig. 5(a) with a green rhombus.

An enumeration of low-energy configurations of a small lattice in order to find a solution for a larger lattice was carried out for a different number of low-energy configurations for each value of parameter c , in order to obtain reliable solutions. We combined pairs of arbitrary low-energy configurations of 20 spins to obtain a configuration for 40 dipoles. Then an enumeration was performed over the selected low-energy configurations of two adjacent combined subsystems, while the energy for the lattice under construction of 40 dipoles was controlled.

The ground state found by means of both the combination method and the complete enumeration method for the system of 40 dipoles is shown in Fig. 7(a). In Fig. 7(b) we have given the excited state for a system of 40 dipoles on the lattice. As in the case of a system of 20 dipoles, the excited state, with

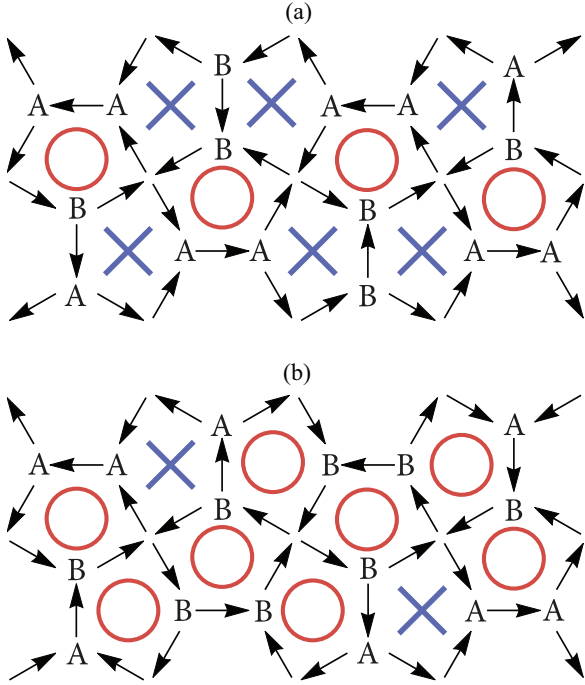


FIG. 7. One of four possible ground states (a) and one of the excited states (b) for systems of 40 dipoles, $c = 376$ nm.

many closed pentagons, with the observance of the ice rule and the quasi-ice rule, is not the ground state. The states of the subsystems of 20 dipoles, from which the excited state of 40 dipoles in Fig. 7(b) is constructed, are shown in Fig. 6(a) as blue squares. Red circles in Fig. 6(a) indicate the states of the subsystems of 20 dipoles from which the ground state of the system of 40 dipoles was constructed. In the short-range model for a system of $N = 40$ Ising dipoles in the ground state the situation with distribution of A and B vertex types is the same as for a system of $N = 20$.

A. Predicted Ground State and Comparison with Experimental Observations

We have constructed the ground state of a system with $N = 80$ spins in the model of long-range interactions (see Fig. 8). We have obtained energies and configurations close to the ground state of a system of 20 dipoles. By a complete enumeration over a given number of low-energy configurations, such states of systems of 20 dipoles were found, from which the ground state 80 is constructed.

It is interesting to note that for $N = 80$, the configurations of the candidate on the ground state for all systems studied by us with $c = 376, 450, 500,$ and 600 nm are the same, except for a few moments on the perimeter having different directions, while all strictly obey all ice-rule constraints.

In the predicted ground state, Fig. 8, we see an arrangement of these vertex types, completely fulfilling the emergent ice rule (two Type A and two Type B). All vertices from four dipoles in the theoretically predicted ground state satisfy the ice rule—“two in” and “two out.”

One of two possible candidates on a ground state for all researched Ising-dipole Cairo lattices in the interval for

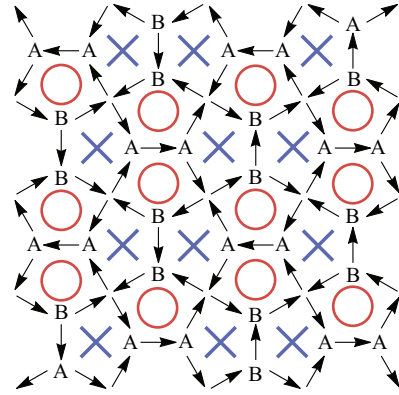


FIG. 8. One of four possible ground-state configurations for a system of 80 dipoles, $c = 376$ nm. The ground state consists of Type I vertices at the four-island vertices, a strict ice-rule obedience at the kagome three-island vertices, and an obedience to the emergent ice rule (two Type A and two Type B vertices) within four-vertex plaquettes [63].

$376 \leq c \leq 600$ nm was obtained by way of the simple translations of the low-energy unit cell presented in Fig. 8. We have calculated the low-energy configuration for $N = 2000$ Ising dipoles (and more)—a candidate on the ground state, therefore, now we are able to obtain the projections S_i to plot the main features of the XMCD contrast. In Fig. 9(a), by the same way as is in Fig. 1(d), the Ising dipole moments S_i were projected onto a given theoretical direction (the direction of the x rays in the experiment), that gave the gray-scale image for the predicted ground state. We have shown in Fig. 9(a) a simulated XMCD snapshot of the configuration of a candidate on the ground state for the $N = 2000$ Ising-like dipoles system on the Cairo pentagonal lattice for $c = 376, 450, 500,$ and 600 nm. This figure is similar to Fig. 4 of [63], where x-ray radiation was directed from left to right at an angle of 17 degrees, with the only difference that we used images without halftones for greater contrast in Fig. 9(a).

To test this ground-state prediction, we aimed at comparing the prediction with experimentally observed low-energy configurations, following a thermal annealing of dipolar Cairo lattices [63]. Electron beam lithography was used to fabricate dipolar Cairo lattices [63]. First, a 70-nm-thick polymethylmethacrylate (PMMA) resist layer was spin-coated on a silicon (100) substrate. Following e-beam exposure and development, a 2.6-nm-thick Permalloy ($\text{Ni}_{80}\text{Fe}_{20}$) thin film was deposited (base pressure: 2×10^{-7} Torr), along with a 2-nm-thick aluminum capping layer to avoid fast oxidation. Lift-off in acetone is then used to remove all of the unwanted magnetic material from the substrate. Taking a background Cairo lattice with lattice parameters $a = 472$ nm and $b = 344$ nm [see Fig. 1(a)], the resulting nanoislands with lengths $L = 300$ nm, widths $W = 100$ nm are then arranged onto the sites of this Cairo lattice. The variation of lattice parameter $c = 376$ nm, 450 nm, 500 nm [see Fig. 1(b)], and 600 nm allows direct control and manipulation of competing dipolar interactions [63]. In accordance with previous work [63,66–68], the thickness and overall dimensions of the nanoislands were chosen to result in a blocking temperature (temperature at which thermally induced moment reorientations occur at a time scale

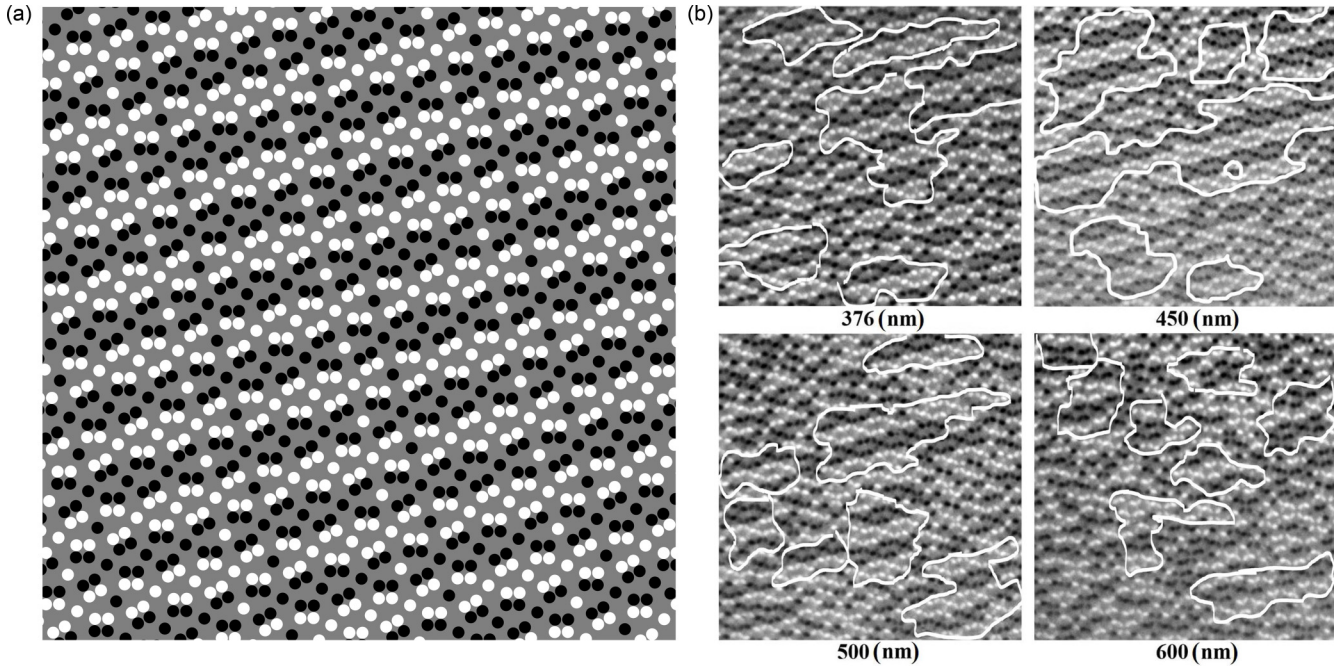


FIG. 9. (a) Simulated XMCD image for the candidate for the ground state of the dipole Cairo lattice for $376 \leq c \leq 600$ nm. (b) Experimentally observed low-energy clusters (ground-state domains) for Cairo lattices with different c .

of a few seconds) around 130 K. Each nanoisland is small enough, to be in the monodomain state, and elongated, so that magnetic moments can only point in one of two possible directions along the long axis of a given nanoisland. Thus, each nanoisland represents a single Ising macrospin. This is the rationale for using the Ising model.

Magnetic imaging was performed using cryogenic photoemission electron microscopy (PEEM) [69], employing x-ray magnetic circular dichroism (XMCD) at the Fe L3 edge [70]. An XMCD image is obtained by a pixel-wise division of images recorded with circular left and right polarized light. The resulting dark and bright contrast is a direct measurement of the orientation of a given magnetic moment with respect to incoming x rays. Moment pointing towards the incoming x rays will appear dark, while moments opposing the incoming x-ray direction will appear bright [see Fig. 9(b)]. Following fabrication, the sample was placed in vacuum at room temperature for seven days, before it was transferred into PEEM for magnetic imaging. In PEEM, the sample was cooled down to 100 K, to ensure that all moments remain frozen during XMCD imaging after this thermal annealing procedure.

The existence of clusters of a low-energy phase, cluster formation, the emergence of a “percolation cluster,” i.e., the processes of merging into one large cluster the connection of clusters (domains) of the ground state with thermodynamics, were discussed for artificial superspin ice in Refs. [29,30], and for macrospin glass in Ref. [71].

In Fig. 9(b), low-energy (ground-state) domains are highlighted by white contours in the experimental XMCD images, where an ordering close to the theoretically predicted one is preferable. The gray-scale contrast on experimental images is more diverse. In Fig. 9(b) for some points, we see weak contrast, because these islands have similar 75° – 80° angles with respect to incoming x rays. Maximum contrast is seen

when we have parallel moments (0 degrees) with respect to incoming x rays. An island with a 90° angle with respect to incoming x rays will show no contrast at all.

For a small number of dipoles on the Cairo lattice in the model of long-range interaction, Figs. 3(b) and 6 show that the configurations of the ground state have a zero value of spin excess $M = 0$. This is logical, since the dipole-dipole interaction has antiferromagnetic nature. Exact calculations show that the situation of $M = 0$ is conserved for lattices with larger size $N = 40$ and 80 . The processing of the experimental data showed that for the researched lattices, the average absolute value of spin excess is $|M|$ per one dipole, as presented in the Table I.

Figure 10 shows the values of the interaction energy in the configurations of the ground state from the lattice parameter c per one dipole for $N = 20, 40, 80$ dipoles. The curves are constructed using the least-squares method. For values $c > 600$, where all systems decay into separate subsystems of $n = 5$ dipoles, the value of the ground-state energy of pentagonal lattices of various numbers of dipoles N tends to the same one for all lattices of a finite number of dipoles under study. The dependence of the reduced ground-state energy on the lattice parameter $\frac{E_{GS}(c)}{DN}$ exhibits a maximum with a further

TABLE I. The average values of spin excess per one dipole for experimental samples.

c (nm)	$ M $ (dimensionless units)
376	0.01948 ± 0.00389
450	0.04544 ± 0.00909
500	0.04578 ± 0.00916
600	0.04093 ± 0.00818

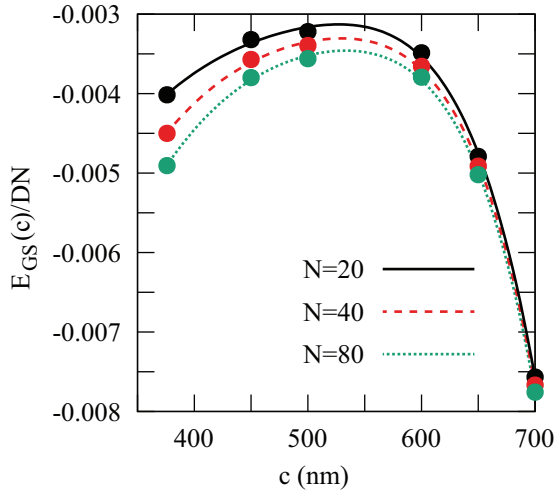


FIG. 10. Normalized energy depending on c , for $N = 20, 40, 80$ dipoles.

decrease in c , i.e., with an increase in the influence of the nearest neighbors, the difference in the ground-state energy of the studied systems with varying numbers of particles becomes essential. This is due to an increase in the interaction energy in the ground state with a decrease in the value of c , which in turn leads to an increase in the contribution to the total interaction energy of the nearest neighbors due to an effective increase in the coordination number, as well as to a decrease in the influence of boundary dipoles, the ratio of the number of which to the total number of dipoles decreases with increasing N . Similar dependencies in the behavior of $\frac{E_{GS}(c)}{DN}$ for a system of 80 dipoles, which were constructed by the combination method and independently found by the Monte Carlo method, as well as systems with the smaller number of 40 and 20 dipoles, which were calculated by the complete enumeration method in Fig. 10, are indirect confirmation of the reliability of the obtained configurations of the ground state of the lattices of 80 dipoles.

Figure 11 shows the values and the dependencies of the frustration parameter on the lattice parameter c calculated by the least-squares method at $T \rightarrow 0$. Our proposed quantitative measure of relative frustration for all explored systems did not exceed 33%. This figure reflects the ratio of the number of excitations to the total number of paired interactions. As one can see, the band gap, i.e., the frustration parameter, behaves nonmonotonically as a function of c : It has a maximum. At very large values of c , all curves are combined into one, since the system splits into “independent pentads.”

Figure 11 presents the results of the calculations of the frustration parameter P_f (relative number of excitations). Experimental data show a larger number of excitations (about 50%) than in the theoretically predicted ground-state configuration (less than 33%) for all studied values of the lattice parameters.

The results presented in Figs. 10 and 11 were obtained for systems of a finite number of Ising dipoles located on the pentagonal Cairo lattice. A characteristic property of this lattice is that the special geometry of the pentagonal lattice with a change in one of the lattice parameters (number of

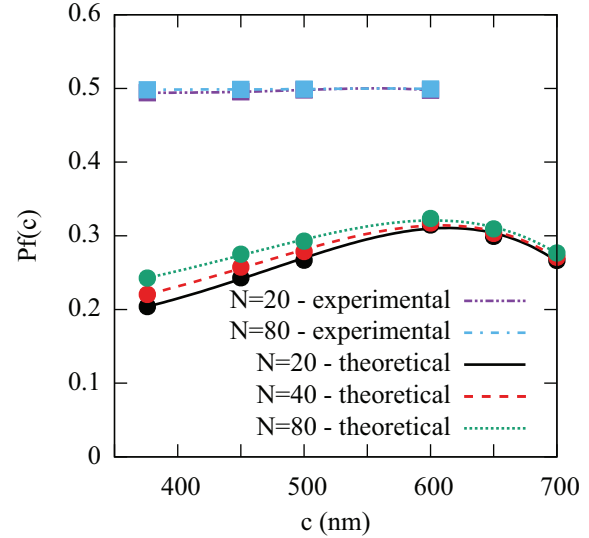


FIG. 11. The frustration parameter for systems with $N = 20, 40, 80$ at $c = 376, 450, 500, 600, 650, 700$ nm (theoretical data, circle points) and for systems with $N = 20, 80$ at $c = 376, 450, 500, 600$ nm (experimental data, square points).

nearest neighbors) leads to a change in the level of geometric frustrations.

For the comparison of the considered systems, for the analysis, and for the conclusions about the ground-state energy in the thermodynamic limit, the finite-dimensional scaling was performed. Our theoretical predictions about the magnetic ordering rules in the ground state allows us to obtain systems with a relatively large number of Ising dipoles. Regions containing different numbers of dipoles were taken on experimental XMCD pictures; the reverse operation of the conversion was performed of the black-and-white contrast

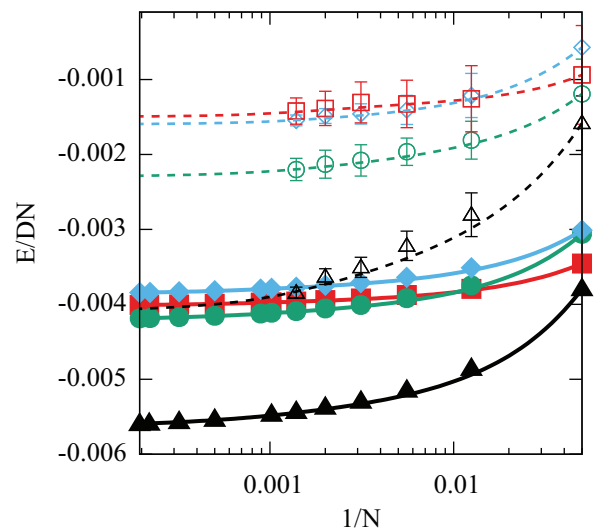


FIG. 12. Scaling of the final size for theoretically calculated candidates in the ground state (solid curves) and for experimental data (dashed lines with error bars). Colored lines with black triangles, green circles, blue diamonds, and red squares refer to the lattice parameter values $c = 376, 450, 500$, and 600 nm, respectively.

to the corresponding values of S_i at known coordinates and magnetic moments, which made it possible to calculate the energy of the dipole-dipole interaction. We have presented the results of extrapolation with finite-size scaling for comparison both for the theoretically calculated ground-state energy and for experimental XMCD data in Fig. 12.

The standard deviation from the mean lines is that there is a spread in energies depending on the selection of the site. It took place because the experimental XMCD images show significant order violations for the predicted ground state. In the model of long-range dipole-dipole interaction, the low-energy states obtained experimentally (Fig. 9) have an energy higher than that theoretically calculated for both researched values of lattice parameter c . The mean lines were computed using the GNU PLOT program package smoothing method.

IV. CONCLUSIONS

We calculated all possible configurations for systems of 20 and 40 Ising-like dipoles on the Cairo lattice by means of the enumeration method. It is possible to exactly find all ground states for the investigated images of the Cairo pentagonal lattices with the parameter $c = 376, 450, 500,$ and 600 nm. The results obtained for $N = 40$ made it possible to test and debug the Monte Carlo and combination methods that were used to construct lattices of $N = 80$ dipoles and to make assumptions about the configuration of the ground state.

Identical results were found by independent calculations of the ground-state configurations using the Monte Carlo method and the combination method, which is consistent evidence that the ground-state configuration for the Cairo lattice of 80 dipoles has been found. The reliability of the results is also confirmed by the fact that they have the same type of dependencies on c and N of the energy and the frustration parameter for the Cairo pentagonal lattices.

Comparison of the theoretically predicted ground state and the experimentally obtained low-energy states showed that in the experiment, clusters of the ground state are observed [see Fig. 9(b)]. It is obvious that the experimental system attempts to access a long-range ordered ground state, but as shown in previous studies on various artificial frustrated spin systems, fabrication-related intrinsic disorder, and the blocking temperature of the nanomagnets can significantly slow down and hinder relaxation towards a long-range ordered ground state [64,65,68]. The free energy minimum must correspond to stable thermodynamic equilibrium and the realization of the most probable state. For the temperature range below the blocking temperature, reaching the equilibrium state during the experiment can be difficult, for example, due to the hierarchical distribution of logarithmic-large relaxation times.

It is shown that the dependence on c of the ground-state energy of the Cairo pentagonal lattices exhibits a nonmonotonic behavior, thus the lattice parameters can be used to control the geometric frustration. For Cairo lattices of dipoles in the

configurations of the ground states, the quantity of closed pentagons is less than maximally possible. Configurations with more closed pentagons have higher interaction energy. The ordering in the configurations of the ground states obeys the ice rule and the quasi-ice rule.

In this work, for the model of long-range dipole interaction, we tried to investigate the question of the existence of an elementary magnetic cell, which can be translated to obtain the global ground state. In other words, the question of whether there is a translational order in the ground state of the artificial dipole spin ice of the Cairo lattice was investigated. The solution to the problem of the ground state both in the model with a short interaction radius and in the model with a long-range interaction radius rests on the central problem of the theory of algorithms—the problem of P and NP. This is a serious theoretical riddle, the main unsolved problem of computer science.

In the long-range interaction model for the researched system of a finite number of Ising dipoles, there are only two or four opposite configurations of ground states. In the short-range model, it is possible that a macroscopic degeneracy of the ground-state configurations is observed.

In our research, we proceeded from the assumptions that if a system of a relatively large number of particles is in the energy minimum, then the subsystems into which it can be divided should also be in their energy minima, since energy is additive. The excitations from these minima are associated with the influence of the boundaries. Boundary effects should be researched more thoroughly, e.g., it would be interesting to determine the influence of periodic or antiperiodic boundary conditions on the solutions.

Artificial spin ice systems on the Cairo lattice can exhibit exotic thermodynamic properties that would be interesting to study for the development of the theory of phase transitions. We investigated the problem of the configuration of the ground state in a zero external magnetic field. It is of interest to study the behavior of the magnetic susceptibility as a function of temperature, calculate the blocking temperature and Curie temperature, energy, spin excess, and degeneracy of the ground-state configurations in a nonzero external magnetic field.

ACKNOWLEDGMENTS

Part of the work was financially supported by the state task of the Ministry of Science and Higher Education of the Russian Federation Grant No. 075-00400-19-01. A.F. and K.H. received support from the Swiss National Science Foundation (Projects No. 174306 and No. 200020_172774). This research used resources of the Advanced Light Source, a U.S. DOE Office of Science User Facility under Contract No. DE-AC02-05CH11231. The authors express their deep gratitude for the powerful computer technology provided by the Center for Shared Use “Data Center of the Far Eastern Branch of the Russian Academy of Sciences” [72].

[1] G. Wannier, Antiferromagnetism. The triangular Ising net, *Phys. Rev.* **79**, 357 (1950).

[2] J. A. Mydosh, *Spin Glasses: An Experimental Introduction* (CRC Press, Boca Raton, 1993).

- [3] V. Belokon and K. Nefedev, Distribution function for random interaction fields in disordered magnets: Spin and macrospin glass, *J. Exp. Theor. Phys.* **93**, 136 (2001).
- [4] J. D. Bernal and R. H. Fowler, A theory of water and ionic solution, with particular reference to hydrogen and hydroxyl ions, *J. Chem. Phys.* **1**, 515 (1933).
- [5] L. Pauling, The structure and entropy of ice and of other crystals with some randomness of atomic arrangement, *J. Am. Chem. Soc.* **57**, 2680 (1935).
- [6] M. J. Harris, S. T. Bramwell, D. F. McMorrow, T. Zeiske, and K. W. Godfrey, Geometrical Frustration in the Ferromagnetic Pyrochlore $\text{Ho}_2\text{Ti}_2\text{O}_7$, *Phys. Rev. Lett.* **79**, 2554 (1997).
- [7] A. P. Ramirez, A. Hayashi, R. J. Cava, R. Siddharthan, and B. Shastri, Zero-point entropy in 'spin ice', *Nature (London)* **399**, 333 (1999).
- [8] S. T. Bramwell and M. J. Gingras, Spin ice state in frustrated magnetic pyrochlore materials, *Science* **294**, 1495 (2001).
- [9] A. Farhan, M. Saccone, C. F. Petersen, S. Dhuey, R. V. Chopdekar, Y.-L. Huang, N. Kent, Z. Chen, M. J. Alava, T. Lippert, A. Scholl, and S. van Dijken, Emergent magnetic monopole dynamics in macroscopically degenerate artificial spin ice, *Sci. Adv.* **5**, eaav6380 (2019).
- [10] B. Farmer, V. S. Bhat, A. Balk, E. Teipel, N. Smith, J. Unguris, D. J. Keavney, J. T. Hastings, and L. E. De Long, Direct imaging of coexisting ordered and frustrated sublattices in artificial ferromagnetic quasicrystals, *Phys. Rev. B* **93**, 134428 (2016).
- [11] A. Peretyatko, K. Nefedev, and Y. Okabe, Interplay of dilution and magnetic field in the nearest-neighbor spin-ice model on the pyrochlore lattice, *Phys. Rev. B* **95**, 144410 (2017).
- [12] J. Drisko, T. Marsh, and J. Cumings, Topological frustration of artificial spin ice, *Nat. Commun.* **8**, 1 (2017).
- [13] Y. Shevchenko, K. Nefedev, and Y. Okabe, Entropy of diluted antiferromagnetic Ising models on frustrated lattices using the Wang-Landau method, *Phys. Rev. E* **95**, 052132 (2017).
- [14] D. Shi, Z. Budrikis, A. Stein, S. A. Morley, P. D. Olmsted, G. Burnell, and C. H. Marrows, Frustration and thermalization in an artificial magnetic quasicrystal, *Nat. Phys.* **14**, 309 (2018).
- [15] V. Brajuskovic, A. Addi, C. Phatak, and A. K. Petford-Long, Observation of transient states during magnetization reversal in a quasicrystal artificial spin ice, *Phys. Rev. B* **98**, 094424 (2018).
- [16] P. Andriushchenko, K. Soldatov, A. Peretyatko, Y. Shevchenko, K. Nefedev, H. Otsuka, and Y. Okabe, Large peaks in the entropy of the diluted nearest-neighbor spin-ice model on the pyrochlore lattice in a [111] magnetic field, *Phys. Rev. E* **99**, 022138 (2019).
- [17] A. Makarov, K. Makarova, Y. A. Shevchenko, P. Andriushchenko, V. Y. Kapitan, K. Soldatov, A. Perzhu, A. Rybin, D. Y. Kapitan, E. Vasil'ev *et al.*, On the numerical calculation of frustrations in the Ising model, *JETP Lett.* **110**, 702 (2019).
- [18] Y. A. Shevchenko, V. Kapitan, and K. V. Nefedev, Specific heat of square spin ice in finite point Ising-like dipoles model, in *Solid State Phenom.* **245**, 23 (2015).
- [19] R. Silva, F. Nascimento, L. Mól, W. Moura-Melo, and A. Pereira, Thermodynamics of elementary excitations in artificial magnetic square ice, *New J. Phys.* **14**, 015008 (2012).
- [20] J. Porro, A. Bedoya-Pinto, A. Berger, and P. Vavassori, Exploring thermally induced states in square artificial spin-ice arrays, *New J. Phys.* **15**, 055012 (2013).
- [21] I. Gilbert, G.-W. Chern, S. Zhang, L. O'Brien, B. Fore, C. Nisoli, and P. Schiffer, Emergent ice rule and magnetic charge screening from vertex frustration in artificial spin ice, *Nat. Phys.* **10**, 670 (2014).
- [22] A. Farhan, A. Scholl, C. F. Petersen, L. Anghinolfi, C. Wuth, S. Dhuey, R. V. Chopdekar, P. Mellado, M. J. Alava, and S. Van Dijken, Thermodynamics of emergent magnetic charge screening in artificial spin ice, *Nat. Commun.* **7**, 12635 (2016).
- [23] G.-W. Chern and P. Mellado, Magnetic monopole polarons in artificial spin ices, *Europhys. Lett.* **114**, 37004 (2016).
- [24] A. Ortiz-Ambriz, C. Nisoli, C. Reichhardt, C. J. O. Reichhardt, and P. Tierno, Colloquium: Ice rule and emergent frustration in particle ice and beyond, *Rev. Mod. Phys.* **91**, 041003 (2019).
- [25] L. J. Heyderman and R. L. Stamps, Artificial ferroic systems: Novel functionality from structure, interactions and dynamics, *J. Phys.: Condens. Matter* **25**, 363201 (2013).
- [26] C. Nisoli, R. Moessner, and P. Schiffer, Colloquium: Artificial spin ice: Designing and imaging magnetic frustration, *Rev. Mod. Phys.* **85**, 1473 (2013).
- [27] C. Nisoli, Frustration (s) and the ice rule: From natural materials to the deliberate design of exotic behaviors, in *Frustrated Materials and Ferroic Glasses* (Springer, Berlin/Heidelberg, 2018), pp. 57–99.
- [28] P. E. Lammert, X. Ke, J. Li, C. Nisoli, D. M. Garand, V. H. Crespi, and P. Schiffer, Direct entropy determination and application to artificial spin ice, *Nat. Phys.* **6**, 786 (2010).
- [29] Y. Shevchenko, A. Makarov, and K. Nefedev, Effect of long- and short-range interactions on the thermodynamics of dipolar spin ice, *Phys. Lett. A* **381**, 428 (2017).
- [30] Y. A. Shevchenko, A. Makarov, P. Andriushchenko, and K. Nefedev, Multicanonical sampling of the space of states of $H(2,n)$ -vector models, *J. Exp. Theor. Phys.* **124**, 982 (2017).
- [31] S. H. Skjærvø, C. H. Marrows, R. L. Stamps, and L. J. Heyderman, Advances in artificial spin ice, *Nat. Rev. Phys.* **2**, 13 (2020).
- [32] Y.-L. Wang, Z.-L. Xiao, A. Snezhko, J. Xu, L. E. Ocola, R. Divan, J. E. Pearson, G. W. Crabtree, and W.-K. Kwok, Rewritable artificial magnetic charge ice, *Science* **352**, 962 (2016).
- [33] R. Wang, C. Nisoli, R. S. d. Freitas, J. Li, W. McConville, B. Cooley, M. Lund, N. Samarth, C. Leighton, V. Crespi *et al.*, Artificial 'spin ice' in a geometrically frustrated lattice of nanoscale ferromagnetic islands, *Nature (London)* **439**, 303 (2006).
- [34] S. Ladak, D. Read, G. Perkins, L. Cohen, and W. Branford, Direct observation of magnetic monopole defects in an artificial spin-ice system, *Nat. Phys.* **6**, 359 (2010).
- [35] J. P. Morgan, A. Stein, S. Langridge, and C. H. Marrows, Thermal ground-state ordering and elementary excitations in artificial magnetic square ice, *Nat. Phys.* **7**, 75 (2011).
- [36] A. Farhan, P. Derlet, A. Kleibert, A. Balan, R. Chopdekar, M. Wyss, L. Anghinolfi, F. Nolting, and L. J. Heyderman, Exploring hyper-cubic energy landscapes in thermally active finite artificial spin-ice systems, *Nat. Phys.* **9**, 375 (2013).
- [37] S. F. Edwards and P. W. Anderson, Theory of spin glasses, *J. Phys. F* **5**, 965 (1975).
- [38] D. Sherrington and S. Kirkpatrick, Solvable Model of a Spin-Glass, *Phys. Rev. Lett.* **35**, 1792 (1975).
- [39] D. L. Stein and C. M. Newman, *Spin Glasses and Complexity* (Princeton University Press, Princeton, 2013), Vol. 4.

- [40] A. Percus, G. Istrate, and C. Moore, *Computational Complexity and Statistical Physics* (Oxford University Press USA, New York, 2006).
- [41] F. Barahona, R. Maynard, R. Rammal, and J.-P. Uhry, Morphology of ground states of two-dimensional frustration model, *J. Phys. A: Math. Gen.* **15**, 673 (1982).
- [42] C. Newman and D. Stein, Are there incongruent ground states in 2D Edwards-Anderson spin glasses? *Commun. Math. Phys.* **224**, 205 (2001).
- [43] F. Tanaka and S. Edwards, Analytic theory of the ground state properties of a spin glass. I. Ising spin glass, *J. Phys. F* **10**, 2769 (1980).
- [44] J. Avron, G. Roepstorff, and L. Schulman, Ground state degeneracy and ferromagnetism in a spin glass, *J. Stat. Phys.* **26**, 25 (1981).
- [45] N. Metropolis, A. W. Rosenbluth, M. N. Rosenbluth, A. H. Teller, and E. Teller, Equation of state calculations by fast computing machines, *J. Chem. Phys.* **21**, 1087 (1953).
- [46] R. H. Swendsen and J.-S. Wang, Replica Monte Carlo Simulation of Spin-Glasses, *Phys. Rev. Lett.* **57**, 2607 (1986).
- [47] R. H. Swendsen and J.-S. Wang, Nonuniversal Critical Dynamics in Monte Carlo Simulations, *Phys. Rev. Lett.* **58**, 86 (1987).
- [48] F. Wang and D. P. Landau, Efficient, Multiple-Range Random Walk Algorithm to Calculate the Density of States, *Phys. Rev. Lett.* **86**, 2050 (2001).
- [49] K. Soldatov, K. Nefedev, V. Y. Kapitan, and P. Andriushchenko, Approaches to numerical solution of 2D Ising model, *J. Phys.: Conf. Ser.* **741**, 012199 (2016).
- [50] G. Wysin, A. Pereira, W. Moura-Melo, and C. de Araujo, Order and thermalized dynamics in Heisenberg-like square and kagome spin ices, *J. Phys.: Condens. Matter* **27**, 076004 (2015).
- [51] R. Moessner and S. L. Sondhi, Ising models of quantum frustration, *Phys. Rev. B* **63**, 224401 (2001).
- [52] V. Urumov, Exact solution of the Ising model on a pentagonal lattice, *J. Phys. A: Math. Gen.* **35**, 7317 (2002).
- [53] A. Ralko, Phase diagram of the Cairo pentagonal XXZ spin-1/2 magnet under a magnetic field, *Phys. Rev. B* **84**, 184434 (2011).
- [54] E. Ressouche, V. Simonet, B. Canals, M. Gospodinov, and V. Skumryev, Magnetic Frustration in an Iron-Based Cairo Pentagonal Lattice, *Phys. Rev. Lett.* **103**, 267204 (2009).
- [55] I. Rousochatzakis, A. M. Läuchli, and R. Moessner, Quantum magnetism on the Cairo pentagonal lattice, *Phys. Rev. B* **85**, 104415 (2012).
- [56] A. M. Abakumov, D. Batuk, A. A. Tsirlin, C. Prescher, L. Dubrovinsky, D. V. Sheptyakov, W. Schnelle, J. Hadermann, and G. Van Tendeloo, Frustrated pentagonal Cairo lattice in the non-collinear antiferromagnet $\text{Bi}_4\text{Fe}_5\text{O}_{13}\text{F}$, *Phys. Rev. B* **87**, 024423 (2013).
- [57] M. Rojas, O. Rojas, and S. M. de Souza, Frustrated Ising model on the Cairo pentagonal lattice, *Phys. Rev. E* **86**, 051116 (2012).
- [58] A. A. Tsirlin, I. Rousochatzakis, D. Filimonov, D. Batuk, M. Frontzek, and A. M. Abakumov, Spin-reorientation transitions in the Cairo pentagonal magnet $\text{Bi}_4\text{Fe}_5\text{O}_{13}\text{F}$, *Phys. Rev. B* **96**, 094420 (2017).
- [59] G. Möller and R. Moessner, Magnetic multipole analysis of kagome and artificial spin-ice dipolar arrays, *Phys. Rev. B* **80**, 140409(R) (2009).
- [60] G.-W. Chern, P. Mellado, and O. Tchernyshyov, Two-Stage Ordering of Spins in Dipolar Spin Ice on the Kagome Lattice, *Phys. Rev. Lett.* **106**, 207202 (2011).
- [61] C. Castelnovo, R. Moessner, and S. L. Sondhi, Magnetic monopoles in spin ice, *Nature (London)* **451**, 42 (2008).
- [62] L. Anghinolfi, H. Luetkens, J. Perron, M. G. Flokstra, O. Sendetskyi, A. Suter, T. Prokscha, P. Derlet, S. Lee, and L. Heyderman, Thermodynamic phase transitions in a frustrated magnetic metamaterial, *Nat. Commun.* **6**, 8278 (2015).
- [63] M. Saccone, K. Hofhuis, Y.-L. Huang, S. Dhuey, Z. Chen, A. Scholl, R. V. Chopdekar, S. van Dijken, and A. Farhan, Dipolar Cairo lattice: Geometrical frustration and short-range correlations, *Phys. Rev. Materials* **3**, 104402 (2019).
- [64] A. Farhan, P. M. Derlet, A. Kleibert, A. Balan, R. V. Chopdekar, M. Wyss, J. Perron, A. Scholl, F. Nolting, and L. J. Heyderman, Direct Observation of Thermal Relaxation in Artificial Spin Ice, *Phys. Rev. Lett.* **111**, 057204 (2013).
- [65] K. Hofhuis, A. Hrabec, H. Arava, N. Leo, Y.-L. Huang, R. V. Chopdekar, S. Parchenko, A. Kleibert, S. Koraltan, C. Abert, C. Vogler, D. Suess, P. M. Derlet, and L. J. Heyderman, Thermally superactive artificial kagome spin ice structures obtained with the interfacial Dzyaloshinskii-Moriya interaction, *Phys. Rev. B* **102**, 180405(R) (2020).
- [66] M. Saccone, A. Scholl, S. Velten, S. Dhuey, K. Hofhuis, C. Wuth, Y.-L. Huang, Z. Chen, R. V. Chopdekar, and A. Farhan, Towards artificial Ising spin glasses: Thermal ordering in randomized arrays of Ising-type nanomagnets, *Phys. Rev. B* **99**, 224403 (2019).
- [67] M. Saccone, K. Hofhuis, D. Bracher, A. Kleibert, S. van Dijken, and A. Farhan, Elevated effective dimension in tree-like nanomagnetic Cayley structures, *Nanoscale* **12**, 189 (2020).
- [68] A. Farhan, M. Saccone, C. F. Petersen, S. Dhuey, K. Hofhuis, R. Mansell, R. V. Chopdekar, A. Scholl, T. Lippert, and S. van Dijken, Geometrical Frustration and Planar Triangular Antiferromagnetism in Quasi-Three-Dimensional Artificial Spin Architecture, *Phys. Rev. Lett.* **125**, 267203 (2020).
- [69] A. Doran, M. Church, T. Miller, G. Morrison, A. T. Young, and A. Scholl, Cryogenic PEEM at the advanced light source, *J. Electron Spectrosc. Relat. Phenom.* **185**, 340 (2012).
- [70] J. Stöhr, Y. Wu, B. Hermsmeier, M. Samant, G. Harp, S. Koranda, D. Dunham, and B. Tonner, Element-specific magnetic microscopy with circularly polarized x-rays, *Science* **259**, 658 (1993).
- [71] K. Nefedev, M. Savunov *et al.*, Finite interaction range spin glass in the Ising model, *Phys. Solid State* **48**, 1746 (2006).
- [72] A. Sorokin, S. Makogonov, and S. Korolev, The information infrastructure for collective scientific work in the Far East of Russia, *Sci. Tech. Inf. Process.* **44**, 302 (2017).